Cargo adaptor identity controls the mechanism and kinetics of dynein activation

Received for publication, October 11, 2024, and in revised form, January 22, 2025 Published, Papers in Press, February 26, 2025,
https://doi.org/10.1016/j.jbc.2025.108358

John P. Gillies[1,‡], Saffron R. Little[1,‡], Aravintha Siva[1], William O. Hancock[2], and Morgan E. DeSantis[1,*]
From the [1]Department of Molecular, Cellular, and Developmental Biology, University of Michigan, Ann Arbor, Michigan, USA; [2]Departments of Biomedical Engineering and Chemistry, Pennsylvania State University, University Park, Pennsylvania, USA

Reviewed by members of the JBC Editorial Board. Edited by Enrique De La Cruz

Cytoplasmic dynein-1 (dynein), the primary retrograde motor in most eukaryotes, supports the movement of hundreds of distinct cargos, each with specific trafficking requirements. To achieve this functional diversity, dynein must bind to the multi-subunit complex dynactin and one of a family of cargo adaptors to be converted into an active, processive motor complex. Very little is known about the dynamic processes that promote the formation of this complex. To delineate the kinetic steps that lead to dynein activation, we developed a single-molecule fluorescence assay to visualize the real-time formation of dynein-dynactin-adaptor complexes *in vitro*. We found that dynactin and adaptors bind dynein independently rather than cooperatively. We also found that different dynein adaptors promote dynein-dynactin-adaptor assembly with dramatically different kinetics, which results in complex formation occurring *via* different assembly pathways. Despite differences in association rates or mechanism of assembly, all adaptors tested can generate a population of tripartite complexes that are very stable. Our work provides a model for how modulating the kinetics of dynein-dynactin-adaptor binding can be harnessed to promote differential dynein activation and reveals a new facet of the functional diversity of the dynein motor.

Cytoplasmic dynein-1 (dynein) is a 1.5 MDa motor protein complex that uses energy derived from ATP hydrolysis to move processively toward the minus-end of the microtubule (1). A single dynein motor complex contains two copies each of six different subunits (Fig. 1*A*) (2). In all eukaryotes, except land plants, dynein is responsible for most long-distance retrograde cargo trafficking (3). Dynein also has essential roles in building and aligning the mitotic spindle and promoting the metaphase-anaphase transition by silencing the Spindle Assembly Checkpoint (1). To support these diverse functions, dynein interacts with a network of regulatory proteins. In fact, dynein is unable to bind cargo or move processively on the microtubule unless it is in complex with the multi-subunit complex, dynactin, and one of a family of cargo adaptors (4). The complex of dynein-dynactin-adaptor, which we will refer to as the *activated transport complex*, is the functional unit that is responsible for dynein-driven cargo motility (Fig. 1*A*) (5, 6). There are nearly 20 identified adaptors in humans, many of which localize to distinct cargos (4). This means that adaptors are responsible, in part, for dynein's ability to traffic cargo with specificity. How dynein discriminates between adaptors to bind to specific cargos remains an outstanding question.

Multiple structural and biochemical studies have revealed how dynactin and an adaptor convert dynein from an autoinhibited conformation, called Phi, to an active and processive motor (Fig. 1*A*) (5–11). In the Phi conformation, the motor domains are held in a crossed conformation that results in a low affinity, non-productive interaction between dynein and the microtubule track (10). In contrast, in the activated transport complex, dynein's motors are in a parallel conformation, which places both microtubule binding domains in the same orientation and allows the motor domain to productively hydrolyze ATP (7, 8, 11). These conformational changes are driven by extensive interactions that occur between multiple dynein subunits, dynactin subunits, and the adaptor (Fig. 1*A*).

Despite knowing its final structure, we know almost nothing about the dynamic processes that govern how the activated transport complex forms. Elucidating the mechanism of how dynein binds to dynactin and adaptor is essential as dynein activation is the direct outcome of the formation of this complex. To address this gap and uncover the mechanism of how dynein-dynactin-adaptor binding occurs, we developed a single-molecule based assay to monitor complex formation in real time using Total Internal Reflection Fluorescence (TIRF) microscopy. We found that different adaptors assemble into the activated transport complex with different kinetics and *via* a different mechanism, but that once formed, all adaptors tested can form very stable, long-lived activated transport complexes. We also found that the order of complex assembly can influence the resultant complex stability. These findings suggest that differences in dynein-dynactin-adaptor binding kinetics or assembly mechanisms may contribute to how dynein achieves adaptor binding specificity in cells and helps to explain the diversity of dynein function.

‡ These authors contributed equally to this work.
* For correspondence: Morgan E. DeSantis, mdesant@umich.edu.

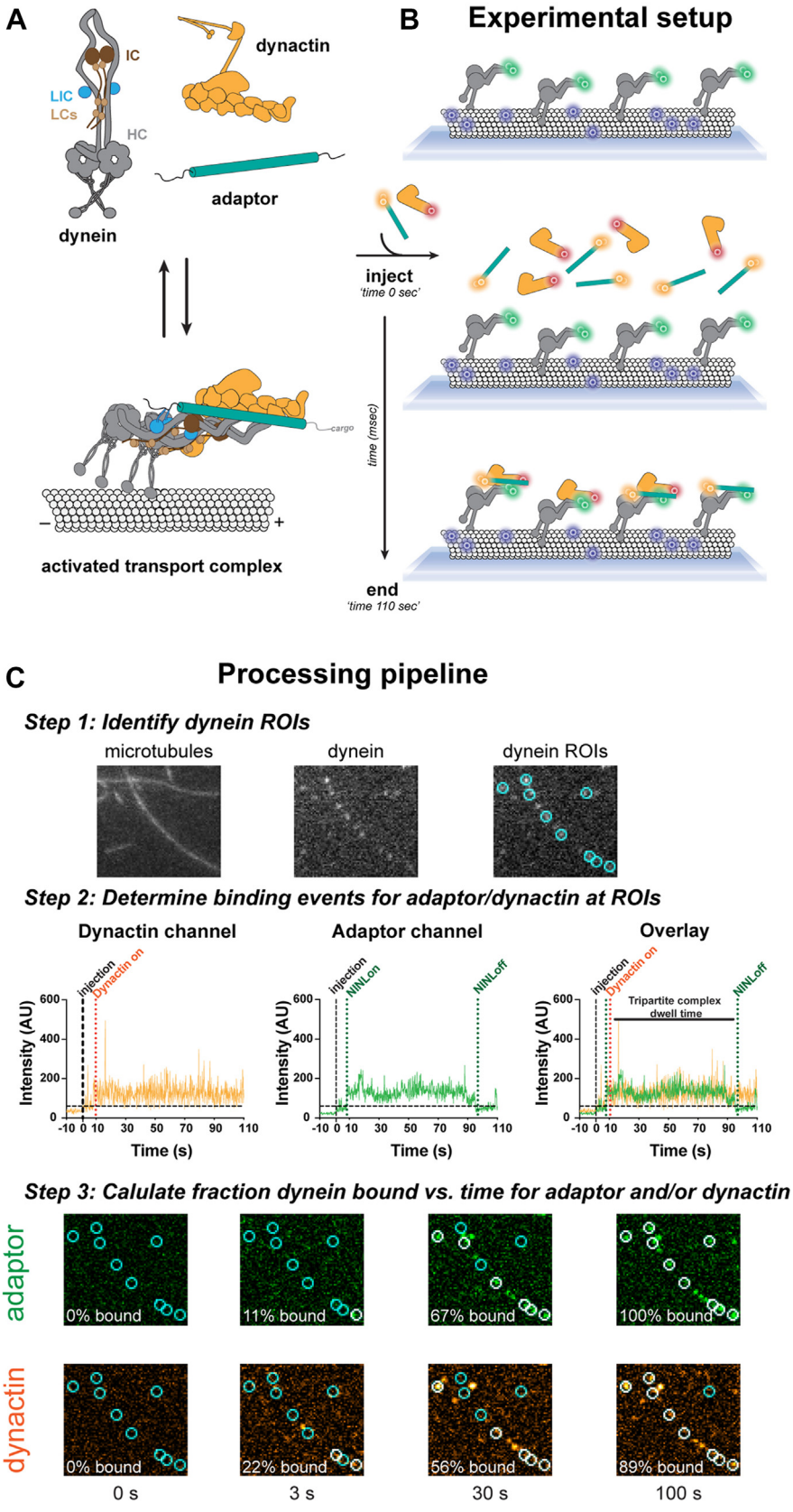

Figure 1. Single molecule association assay development to study dynein binding kinetics. *A*, diagram of dynein activation. Dynein (heavy chain (HC): *gray*; intermediate chain (IC): *dark brown*; light intermediate chain (LIC): *blue*; light chains (LCs): *light brown*) must bind to dynactin (*yellow*) and adaptor (*teal*) to form an activated transport complex capable of motility on a microtubule. *B*, experimental setup. Dynein is tightly associated with microtubules, after which dynactin and/or adaptor are flowed in and the intensity of fluorescence is monitored at dynein puncta. *C*, processing pipeline. Step 1: ROIs were generated at individual dynein spots. *Cyan circles* represent selected dynein ROIs. Step 2: The fluorescence intensity of adaptor and/or dynactin was

Results

Single-molecule association assay development

Most of what we know about dynein's association with dynactin and adaptors has been obtained *via* motility experiments that are performed without consideration of the effect of binding kinetics. In these types of studies, dynein, dynactin, and adaptors are mixed; allowed to incubate; and the motility of the resultant complexes is visualized in movies obtained *via* TIRF microscopy. While this approach is powerful because it allows for the quantification of how the assembled activated transport complexes move on the microtubule track, these motility assays cannot return information about how the activated transport complex forms. Further, while these assays indirectly probe the result of complex formation (motility), they do not directly report on dynein's affinity for dynactin or adaptor or relay information about the stability of the formed complex. Additionally, traditional motility experiments cannot address whether dynactin or the adaptor must bind first to form the activated transport complex, or whether the identity of different adaptors bias activated complexes to form through different mechanisms of assembly.

The aim of this study was to obtain information about the dynamic processes that underly dynein activation. Specifically, we set out to address two key questions: 1) *Does the activated transport complex assemble via an ordered or random mechanism?* 2) *Do different adaptors form activated transport complexes with different kinetics or order of assembly?* To answer these questions, we developed a single-molecule assay to visualize dynein-dynactin-adaptor association in real time using TIRF microscopy (Fig. 1, *B* and *C*). First, Alexa-488-labeled dynein was incubated with preassembled Alexa-405-labeled microtubules in a flow chamber (Fig. 1*B*). We included the nucleotide hydrolase apyrase in the binding buffer to ensure that ATP carried over from the purification was depleted, and dynein remained in the apo conformation, which has a high affinity for microtubules. Next, using a custom-built apparatus that allowed us to simultaneously image and inject sample, we flowed in fluorescently labeled dynactin and adaptor and acquired movies of dynactin and adaptor interacting dynamically with dynein at a frame rate of 150 ms/frame (Fig. 1*B*).

To quantify binding kinetics, we monitored dynactin and adaptor intensity over time at dynein puncta, which allowed us to semi-automate the analysis. To accomplish this, we first identified regions of interest (ROIs) as dynein puncta colocalized with microtubules that were present in the first and last frame (Fig. 1*C*- Step 1). We then simultaneously monitored the intensity of the dynactin and/or adaptor fluorophores at the dynein ROIs (Fig. 1*C*- Step 2). Potential binding events were defined as positive deviations in intensity from baseline (as determined after rolling ball background subtraction of each frame), while unbinding events were defined by an elevated intensity returning to baseline (Fig. 1*C*- Step 2). Previous studies have shown that the activated transport complex often contains two dynein dimers and can also contain two adaptor dimers (7, 8). An experimental limitation of this assay is that it monitors the association of one dynein dimer with a dynactin complex and one adaptor dimer (Fig. S1, *A–E*). For an extended discussion of this caveat, refer to the Experimental procedures.

The TMR and JF646 dyes used to label dynactin and adaptor inherently blink and photobleach over time (Fig. S1, *F–H*). To increase confidence that transitions between bound and unbound events reflected changes in protein-protein interactions rather than dye blinking, we enforced an 8-frame persistence cutoff, which means that all events had to last longer than 1.2 s to be considered a *bona fide* instance of binding or unbinding (Fig. S1, *F* and *H*). To reduce the effect of photobleaching on our experimental measurements, we limited the duration of our movies to 120 s, a time frame in which greater than 60% of both dyes remained unbleached (Fig. S1*G*). To rule out the possibility that the specific dyes used on dynactin or adaptors affected the kinetics, most experiments in this study were collected with biological replicates where the identity of the dyes on dynactin and adaptor were swapped.

This assay can yield many kinetic parameters. Association rate constants can be extracted from the binding curves of the fraction of dynein ROIs colocalized with dynactin and/or adaptor over time under different experimental conditions (Fig. 1C- Step 3). By monitoring both dynactin and adaptor channels simultaneously, we can also extract which component associates with dynein first at individual dynein ROIs (Fig. 1*C*- Step 2). Off-rates can be calculated directly by determining the number of unbinding events divided by the total time dynein molecules are bound to dynactin and/or adaptor. Finally, complex stability can also be assessed by measuring the dwell time of complexes formed at each dynein ROI (Fig. 1*C*- Step 2).

NINL and dynactin bind dynein independently

We next set out to establish that the single molecule association assay we developed could report on dynein's association with dynactin and the adaptor NINL, which is proposed to link dynein to MICAL3-RAB8A vesicles and melanosomes (12, 13). When not bound to cargo, many adaptors assume a folded, autoinhibited conformation in which their C-terminal end folds back to block dynein and dynactin association with the adaptors' N-terminal coiled coil (11, 14, 15). To circumvent

measured at dynein ROIs over time. Some kinetic parameters that can be extracted from intensity values (association time and dwell time) are indicated in the figure. These signals were compared to a baseline value to determine when dynactin and adaptor were bound to dynein. For bimolecular (dynein-dynactin or dynein-adaptor) interactions, the dwell begins when the component binds and ends after dissociation. For tripartite complexes, dwells begin with the second component lands and end when the first component dissociates. Step 3. The fraction of dynein bound to either adaptor or dynactin is determined at each timepoint. Unbound dynein ROIs are shown in cyan, bound ROIs are shown in white. By performing binding experiments at varying concentrations of dynactin and adaptor, multiple binding curves of the fraction of dynein bound to dynactin or adaptor vs time can be generated and fit for k_{obs} values. Resultant k_{obs} values can be plotted *versus* [dynactin] or [adaptor] to determine association rate constants. For a more extended description of this pipeline, refer to the Experimental procedures.

potential adaptor autoinhibition and analyze dynein motility in the absence of cargo, many published motility studies use adaptors with C-terminal truncations. For this study, we used a well-characterized truncation of NINL that robustly activates dynein motility and increases the yield and ease of the NINL protein purification (16, 17).

First, we measured the association kinetics of dynein-NINL in the absence of dynactin and dynein-dynactin in the absence of NINL (Fig. 2, *A–D*, Movies S1, S2, Images S1, and S2). To do this, we varied the concentration of NINL or dynactin between 0.005 and 0.010 μM and then calculated the fraction of dynein bound to NINL or dynactin over time. We ensured that dynein on coverslip was sparse (calculated concentrations of dynein for each kinetic experiment in this study did not exceed 1 pM), meaning that association with dynein does not significantly deplete the solution concentration of dynactin or adaptor. For each experiment, the individual binding curves fit a single exponential, as expected for pseudo-first order binding, and the measured k_{obs} displayed a linear dependence on NINL or dynactin concentrations over the range we explored (Figs. 2, *B* and *D* and S2, *A* and *B*). The measured k_{obs} reflect contributions from both k_{on} and k_{off} because under these conditions k_{obs} = [ligand]*k_{on} + k_{off}, where ligand is either NINL or dynactin (18, 19). As an internal control, we directly measured k_{off} values for the dynein-NINL and dynein-dynactin at each concentration range tested, anticipating that the measured k_{off} values should be independent of NINL or dynactin concentration. Contrary to our expectations, we observed a linear relationship between NINL and dynactin concentration and the measured k_{off} rates, with higher protein concentrations resulting in decreased off-rates (Fig. S2, *C* and *D*). We reasoned that we may be missing *bona fide* unbinding events due to the 1.2 s cut-off imposed in our analysis. If k_{on} rates were sufficiently fast, rapid NINL or dynactin unbinding

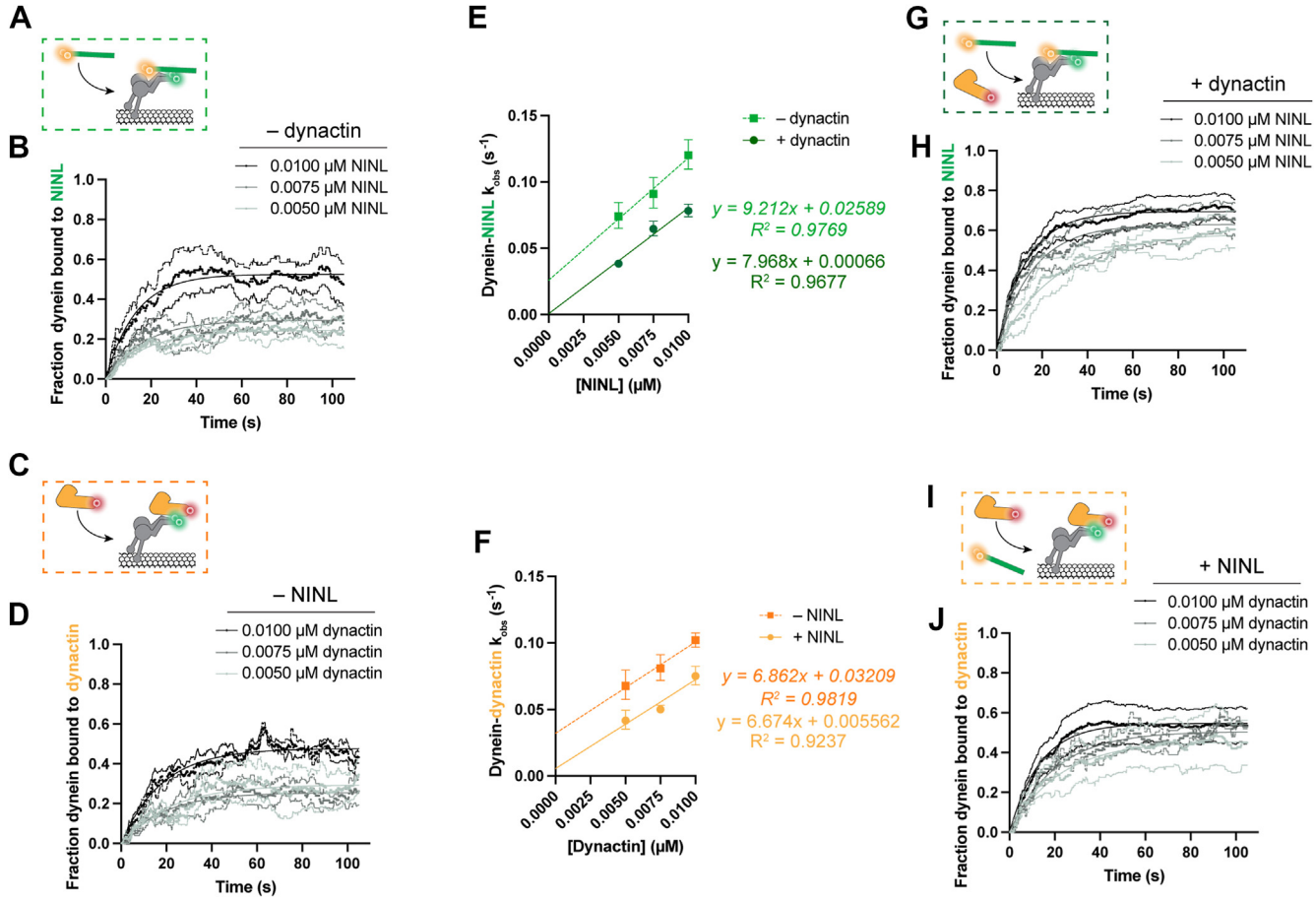

Figure 2. Binding of NINL and dynactin with dynein is not cooperative. *A*, diagram of NINL association with dynein in the absence of dynactin. *B*, fraction of dynein bound to NINL at varied NINL concentrations in the absence of *dynactin*. *Curves* (*solid line*) are fit to a single exponential; *dashed lines* are standard error of the mean. n = 3 for each condition. *C*, diagram of dynactin association with dynein in the absence of NINL. *D*, fraction of dynein bound to dynactin at varied dynactin concentrations in the absence of NINL. Curves (*solid line*) are fit to a single exponential. *dashed lines* are standard error of the mean. n = 3 for each condition. *E*, k_{obs} of NINL binding to dynein at varied NINL concentrations in the presence (*dark green*) or absence (*light green*) of dynactin with corresponding linear regression equations. The data in the absence of dynactin is normalized for the difference in off rates as described in the text. Error bars are 95% confidence intervals. *F*, k_{obs} of dynactin binding to dynein at varied dynactin concentrations in the presence (*yellow*) or absence (*orange*) of NINL with corresponding linear regression equations. The data in the absence of NINL is normalized for the difference in off rates as described in the text. Error bars are 95% confidence intervals. *G*, diagram of NINL association with dynein in the presence of dynactin. *H*, fraction of dynein bound to NINL at varied NINL concentrations in the presence of dynactin. *Curves* (*solid line*) are fit to a single exponential, *dashed lines* are standard error of the mean. n ranges from 3 to 10. *I*, diagram of dynactin association with dynein in the presence of NINL. *J*, fraction of dynein bound to dynactin at varied dynactin concentrations in the absence of NINL. Curves (*solid line*) are fit to a single exponential; *dashed line* is standard error of the mean. n ranges from 3 to 10.

and rebinding could be mistaken for a prolonged binding event. Because k_{on} is concentration dependent, this effect would disproportionately affect experiments with higher protein concentrations. To test this, we repeated the dynein-NINL binding experiment with 0.010 μM NINL, labeling half of the NINL with JF646 and the other with TMR. We observed that the dwell time of dynein colocalized with NINL-JF646 or NINL-TMR was shorter than the measured dwell of dynein colocalized with all NINL, irrespective of dye color, which indicates that rapid unbinding and rebinding is occurring (Fig. S2*E*). In fact, by inspecting individual dynein ROIs, we were also able to directly observe rapid NINL exchange, which would have been missed if both NINL molecules were labeled with the same dye and would have resulted in an erroneously long measured residence time (Fig. S2*F*). Together, these data indicate that rapid rebinding in our assay can result in missed unbinding events and adds concentration-dependent error to the measured k_{obs} values. To correct our k_{obs} values for missed unbinding events, we first fit the measured k_{off} rates to a line to identify the y-intercept as an approximation of the true k_{off} (Fig. S2, *C* and *D*). For dynein-NINL, this value was 0.0627 s^{-1} and for dynein-dyactin it was 0.0817 s^{-1}. Next, we added the difference between the true k_{off} and the measured k_{off} at each concentration of NINL or dynactin to the measured k_{obs} (Fig. 2, *E* and *F*). With this correction, the association rate constant for dynein-NINL was 9.21 μM^{-1} s^{-1} and for dynein-dynactin was 6.86 μM^{-1} s^{-1}.

Next, we set out to measure the kinetics of NINL and dynactin binding to dynein when all three components were present (Fig. 2, *G–J*, Movie S3, and Image S3). To perform these experiments, we varied the concentration of either NINL or dynactin while holding the other constant and monitored the fraction of dynein molecules bound to the variable component over time. It is possible that dynactin and adaptor could interact with each other prior to dynein binding, which would increase the complexity of the reaction scheme and complicate our ability to interpret the measured association rates. To test this possibility, we measured NINL-dynactin binding by a pull-down assay at concentrations 10-fold higher than used in this study and detected no interaction (Fig. S2*G*). Therefore, we did not consider any potential effect of dynactin-adaptor association before dynein binding in these and all following experiments where dynactin and an adaptor were present together.

The resulting binding curves for both dynein-NINL in the presence of dynactin and dynein-dynactin in the presence of NINL fit to single exponentials (Fig. 2, *H* and *J*). Following our previous approach, we next measured the k_{off} rates for dynein-NINL and dynein-dynactin complexes at each concentration tested. Unlike what we observed with the bimolecular binding experiments, the k_{off} values measured when all three components were present did not vary with concentration (Fig. S2, *C* and *D*). Further, the measured k_{off} rates when all components were present were significantly slower than the measured off-rates for either biomolecular experiment (Fig. S2, *C* and *D*). This result indicates that rapid rebinding to dynein did not introduce concentration-dependent error to the k_{obs} for binding experiments performed with all three components. We reason that, because the dissociation rates are significantly slower, the initial complexes formed remain bound for a longer proportion of the experiment and therefore fewer rapid rebinding events erroneously lengthen the apparent complex dwell time.

The k_{obs} for dynein-NINL with dynactin and dynein-dynactin with NINL were linear over the range of concentrations tested and yielded association constants of 7.97 μM^{-1} s^{-1} for dynein-NINL in the presence of dynactin and 6.67 μM^{-1} s^{-1} for dynein-dynactin in the presence of NINL (Fig. 2, *E* and *F*). Importantly, these association rate constants are very similar to those measured for dynein-NINL and dynein-dynactin in the absence of the other binding partner, which indicates that under the conditions of the experiments, NINL and dynactin's association with dynein are likely independent and not cooperative. In other words, NINL and dynactin interact with free dynein at nearly the same rate that they interact with dynein that is already associated with the other partner. These results indicate that, for instance, the binding of one component to dynein does not induce a conformational change that enhances the binding rate of the second component. Moving forward, we will use the average of the association constants measured in the two- and three-component experiments to describe dynein-NINL and dynein-dynactin binding (8.59 μM^{-1} s^{-1} and 6.77 μM^{-1} s^{-1}, respectively).

A population of activated dynein complexes is very long lived

While association rates were similar for both NINL and dynactin in the bimolecular and trimolecular assembly experiments, the measured off-rates were different (Fig. S2, *C* and *D*). To further probe dynein's interaction with NINL or dynactin, we first examined the distributions of dwell times of dynein complexes formed with either 0.010 μM NINL or dynactin in the absence of the other component. While there was a major peak for both dynein-NINL and dynein-dynactin dwell times at ∼5 s, both dwell time distributions were complex and fit best to multiple Gaussians (Fig. 3, *A* and *B*). To more easily quantify the complex stabilities from the measured dwell times, we grouped the measured dwells into three categories: short (events that lasted <20 s), medium (events that lasted 20–80 s), and long (events that lasted >80 s). Dynein-NINL were more stable with 47% of complexes short-lived, 37% medium-lived, and 16% exceeded 80 s (Fig. 3*C*). In contrast, dynein-dynactin bimolecular complexes were less stable, with 69% short-lived, 22% medium-lived, and only 9% long-lived (Fig. 3*D*). Together, these data indicate that dynein's interaction with both NINL and dynactin alone are generally short, with dynein-dynactin events being shorter than dynein-NINL. The observed dwell time differences between NINL and dynactin complexes are also consistent with the off-rates measured and described above (Fig. S2, *C* and *D*). Previous studies that have used separation-based techniques like sucrose gradient ultracentrifugation or size exclusion chromatography have not observed dynein-dynactin complexes form in the absence of adaptor, while we can detect

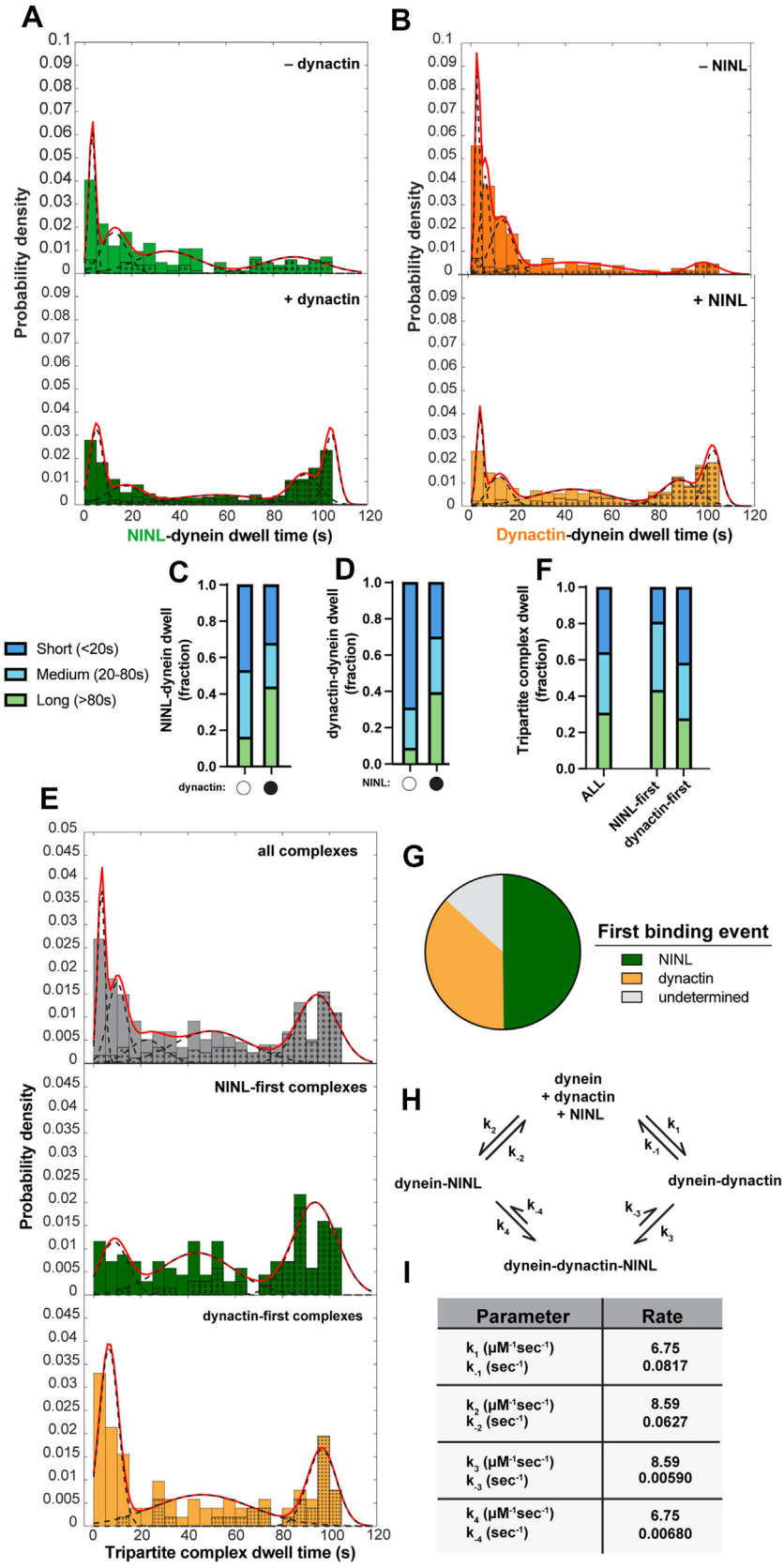

Parameter	Rate
k_1 ($\mu M^{-1}sec^{-1}$) k_{-1} (sec^{-1})	6.75 0.0817
k_2 ($\mu M^{-1}sec^{-1}$) k_{-2} (sec^{-1})	8.59 0.0627
k_3 ($\mu M^{-1}sec^{-1}$) k_{-3} (sec^{-1})	8.59 0.00590
k_4 ($\mu M^{-1}sec^{-1}$) k_{-4} (sec^{-1})	6.75 0.00680

Figure 3. Subpopulations of dynein-dynactin-NINL complexes are very stable and more stable complexes form *via* NINL-first binding events. *A*, histograms of the dwell time of NINL on dynein in the absence (*light green*) and presence (*dark green*) of dynactin. The overall probability density function is shown as a *solid red line*, with individual component Gaussians as *dashed black lines*. *Black dots* show the percentage of the data in each bin that was truncated by the end of the acquisition. *B*, histograms of the dwell time of dynactin on dynein in the absence (*orange*) and presence (*yellow*) of NINL. The overall probability density function is shown as a *solid red line*, with individual component Gaussians as *dashed black lines*. *Black dots* show the percentage of

these short-lived complexes in our assay. One explanation for this difference is that the dynein-dynactin complexes that form on the microtubule in our assay are higher affinity than those formed in solution. It is also possible that dynein-dynactin bimolecular complexes eluded detection in previous assays because of their short dwell times and that dynein-dynactin (and likely dynein-NINL) complexes dissociate too rapidly to be resolved *via* methods not performed at equilibrium (10, 20).

To determine how the presence of the other component alters binding stability of the complexes, we next plotted the dwell time distributions of dynein-NINL and dynein-dynactin obtained from the experiments where both NINL and dynactin were present at 0.010 μM (Fig. 3, *A* and *B*). Like the two component experiments, the dwell time distributions from dynein-NINL and dynein-dynactin complexes formed when all three components were present fit to multiple Gaussians and there was a significant population of short-lived events. However, when all three components were included in the experiment, we observed a dramatic increase in the proportion of long-lived events, with 44% dynein-NINL and 39% dynein-dynactin complexes exceeding 80 s (Fig. 3, *C* and *D*). It is also important to note that nearly 50% of total events were terminated by the movie ending and not by dissociation, which means that the measured dwells are an underestimation of actual dwell times. This observation of long-lived complexes is consistent with the slower k_{off} values measured in experiments when all three components are included (Fig. S2, *C* and *D*).

Despite the clear population of long-lived complexes formed when all three components were present, there was also a population of short-lived binding events (32% and 30% for dynein-NINL and dynein-dynactin, respectively) (Fig. 3, *C* and *D*). From the way that we have conducted the analysis thus far, it is possible that the short-lived dynein-NINL and dynein-dynactin complexes observed in the three component binding experiments could correspond to events where only dynactin or NINL is bound (*i.e.* bimolecular binding events) and that the longer-lived species only occurred when all three components were present at one dynein ROI (*i.e.* tripartite complex formation). To test if this was true, we explicitly extracted dwell times from events only where all three components were colocalized. We observed that dwell times of trimolecular complexes displayed both a short- and long-lived species (Fig. 3, *E* and *F*). This indicates that both low and high stability dynein-dynactin-NINL tripartite complexes can form.

NINL-first binding events favor more stable complexes

An outstanding question is whether there is a required assembly order for forming the activated transport complex. In other words, *is the binding order of dynactin and adaptors to dynein random, or must one of the components bind first?* The measured association rate constants of NINL-dynein and dynactin-dynein are similar, which means that both binding events occur in similar time frames (Fig. 2, *E F*). Because we conducted the trimolecular experiments with fluorophores on both NINL and dynactin, it was possible to monitor each event to determine which component bound first. Consistent with their similar association rates, we observed that 49% of tripartite complexes form NINL-first binding events and 37% form from dynactin-first binding events. (Fig. 3*G*). NINL and dynactin appear to land simultaneously for 13% of tripartite complexes, which is likely a result of the 150 ms detection limit of our movies rather than true simultaneous association, since these proteins don't measurably interact in the absence of dynein (Fig. S2*G*). Importantly, the ratio of NINL-first to dynactin-first events (49%/37% = 1.32) is consistent with what would be predicted from simply considering the ratio of the measured association rate constants (8.59 μM^{-1} s^{-1}/ 6.77 μM^{-1} s^{-1} = 1.27). Together, these data suggest that dynein's association with NINL and dynactin is random and simply governed by their respective association rate constants.

Next, we asked, *does the order of binding influence the stability of the resultant complex?* To answer this, we compared the dwell times of tripartite complexes that formed *via* NINL-first binding events to those that formed *via* dynactin-first binding events. Surprisingly, we found that complexes that formed with NINL binding first were more stable, with 43% of events surviving for greater than 80 s and only 19% of complexes being short-lived. In contrast, only 27% of events that formed with dynactin-first binding survived longer than 80 s, while 41% were short-lived (Fig. 3, *E* and *F*). We interpret this to mean that stable, long-lived dynein-dynactin-NINL complexes are most likely to form when NINL binds first.

Once a tripartite complex is formed, it could disassemble either by dynactin or NINL dissociating first. Thus, next we asked *does the tripartite complex have a preferred pathway for disassembly?* To address this question, we calculated the off-rates of NINL and dynactin from tripartite complexes. We observed no difference in the measured k_{off} for NINL or dynactin's dissociation from the tripartite complex (Fig. S3*A*). This means that once formed, NINL and dynactin are equally likely to unbind from the complex.

With the data we have collected thus far, we can now generate and populate a reaction scheme for the formation of the activated transport complex with dynactin and the adaptor NINL (Fig. 3, *H* and *I*). Our observation that either NINL and dynactin can bind first indicates that the binding reaction is not ordered, and that formation of the complex can proceed

the data in each bin that was truncated by the end of the acquisition. *C* and *D*, fraction of events with dwells that fall into short (<20 s), medium (20–80 s) or long (>80 s) timescales. Fraction shown in (*C*) is calculated from data shown in (*A*); fraction in (*D*) is calculated from data shown in (*B*). *E*, histograms of the dwell time of dynein-dynactin-NINL complexes. All the observed complexes are shown in gray, with the complexes that had NINL bind dynein first in green and the complexes that had dynactin bind dynein first in *yellow*. The overall probability density function is shown as a *solid red line*, with individual component Gaussians as dashed *black lines*. *Black dot* shows the percentage of the data in each bin that was truncated by the end of the acquisition. *F*, fraction of events with dwells that fall into short (<20 s), medium (20–80 s) or long (>80 s) timescales, as calculated from data shown in (*E*). *G*, percentage of complexes that had NINL or dynactin bind dynein first. Undetermined refers to complexes in which NINL and dynactin both bound within one 0.15 s frame. *H*, reaction scheme for the formation of the activated transport complex with dynactin and NINL. *I*, kinetic rates for the reaction scheme in (*H*). The text includes an extended description of the experiments that yielded these rates.

via both arms of the diagram. Because we observe similar rate constants for dynein's association with both partners in bimolecular and trimolecular binding reactions, we can assume that $k_1 = k_4$ and $k_2 = k_3$ (Fig. 3*H*). For these rate constants, we report the average of the association constants measured in the bimolecular and trimolecular experiments (Fig. 2, *E* and *F*). The dissociation rate constants k_{-1} and k_{-2} are extrapolated from the off-rates measured in the bimolecular experiments (Fig. S2, *C* and *D*), and k_{-3} and k_{-4} are calculated directly from the trimolecular binding experiments (Fig. S3*A*).

Adaptor identity controls association kinetics and mechanism of activated dynein complex formation

Different adaptors link dynein to different cargos (4, 17). We hypothesized that different adaptors may support activated transport complex formation with different kinetics. To test this hypothesis, we used the real-time association assay to monitor dynein-dynactin-adaptor complex formation with the adaptor BicD2, which links the dynein transport machinery to Golgi derived vesicles and the nuclear pore complex (20–24). Here, we used a well-characterized C-terminal truncation of BicD2 that prevents autoinhibition (16). In traditional motility assays performed at equilibrium, both NINL and BicD2 promote robust formation of activated transport complexes that move processively along microtubules with similar velocities (16, 25). In contrast, we found that in the real-time association assay, NINL and BicD2 behaved quite differently. In the absence of dynactin, there was almost no measurable binding between dynein and 0.010 μM BicD2 (Fig. S4*A*). The few dynein-BicD2 binding events that did occur were short lived, with a measured off-rate of 0.137 s^{-1} (Figs 4, *A* and *B* and S4*B*).

Next, we monitored dynein-BicD2 association in the presence of 0.010 μM dynactin (Movie S4 and Image S4). Although we observed modest association of BicD2 with dynein in these conditions, the fraction of dynein molecules bound by the end of data acquisition never exceeded ∼25% (Fig. S4*C*). For comparison, ∼60% of dynein molecules were bound to NINL under identical conditions (Fig. 2*B*). Similarly, dynein-BicD2 complexes that formed in the presence of dynactin were less stable, with 72% of complexes being short-lived, 22% medium-lived, and only 6% long-lived (Fig. 4, *A* and *B*). This is in contrast to dynein-NINL complexes, in which over 44% percent had dwells longer than 80 s in the presence of 0.010 μM dynactin (Fig. 3, *A* and *C*). A similar trend was observed in the distributions of dwell times for

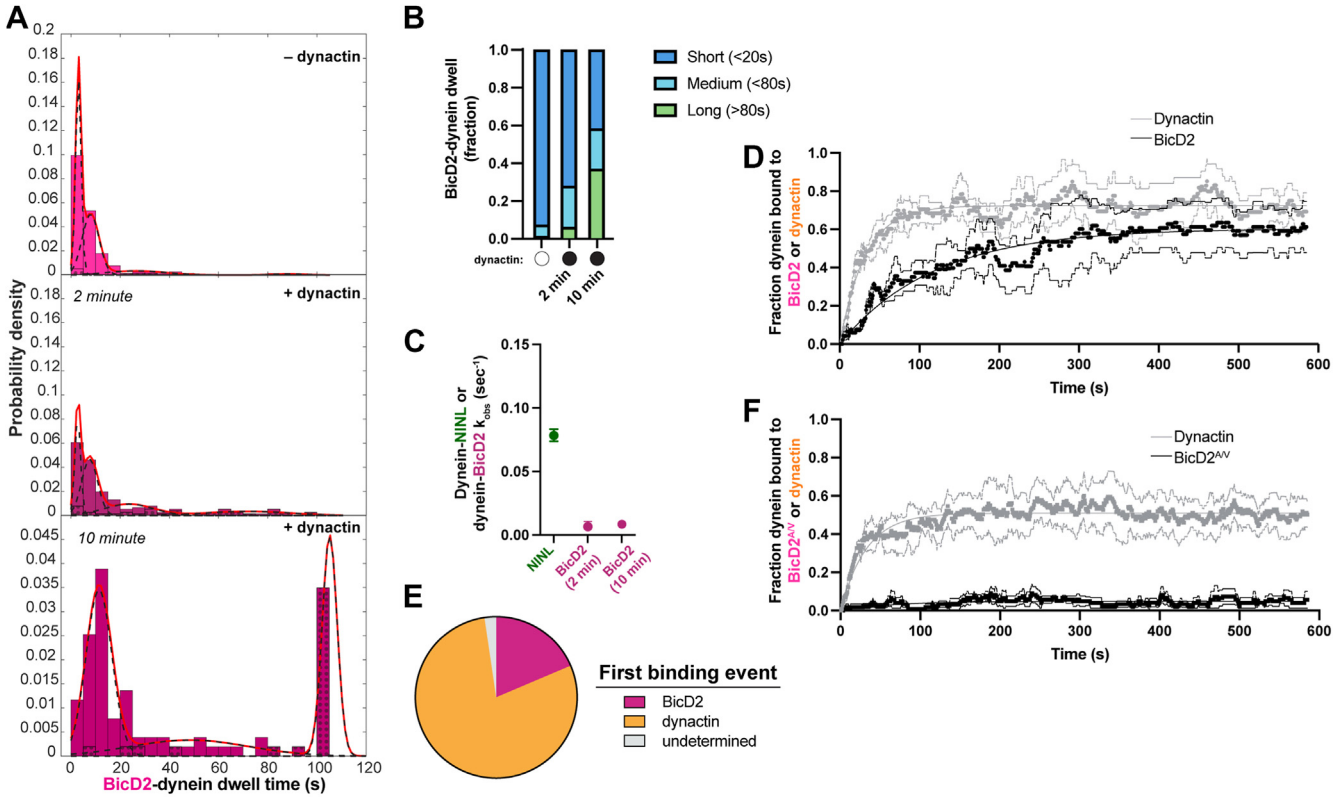

Figure 4. Adaptor identity controls the assembly kinetics of dynein activated transport complexes. *A*, histograms of the dwell time of BicD2 on dynein in the absence (*light pink*) and presence (*dark pink*) of dynactin. Data in the presence of dynactin was collected for 2 min at 0.15 s/frame and at 10 min at 0.75 s/frame. For the 10-min data any dwell times greater than 110 s were randomly given a value between 100 to 110 and marked as censored for this histogram to better compare to the 2-min data. Overall probability density function is shown as a *solid red line*, with individual component Gaussians as *dashed black lines*. *Black dots* show the percentage of the data in each bin that was truncated by the end of the acquisition. *B*, events with dwells times from (*B*) that falls into short (<20 s), medium (20–80 s) or long (>80 s) timescales, calculated from data shown in (*A*). *C*, k_{obs} for dynein-NINL and dynein-BicD2 in the presence of dynactin. NINL data repeated from Figure 2*B*. Error bars represent 95% confidence interval. *D*, fraction of dynein bound to BicD2 in the presence of dynactin over 10 min. *Curve* (*solid line*) is fit to a single exponential, *dashed line* is standard error of the mean. n = 3. *E*, percentage of complexes that had BicD2 or dynactin bind dynein first. *F*, fraction of dynein bound to $BicD2^{A/V}$ in the presence of dynactin over 10 min. Curve (*solid line*) is fit to a single exponential, *dashed line* is standard error of the mean. n = 3.

dynein-dynactin-BicD2 tripartite complexes (Fig. S4, *D* and *E*). Consistent with these observations, the off-rate of dynein-Bicd2 complexes in the presence of dynactin (0.03799 s^{-1}) was much faster than the equivalent measurement with NINL (0.00803 s^{1}) (Figs. S2*C* and S4*B*). Because BicD2 displayed such poor binding to dynein at concentrations amenable to single-molecule analysis, we were unable to determine a dynein-BicD2 association rate constant. However, the k_{obs} for dynein-BicD2 binding in the presence of dynactin is an order of magnitude less than the k_{obs} for NINL in equivalent conditions (Fig. 4*C*).

These data suggest that BicD2 binds slower and forms less long-lived complexes with dynein than NINL. This result also suggests that the 2-min duration of our association experiment may be too short to observe appreciable BicD2 binding. Thus, we repeated the real-time association assay with BicD2 and dynactin but allowed binding to occur over a 10-minute period. To minimize bleaching, we imaged every 750 ms rather than every 150 ms. Consistent with slower binding, experimenting over a period of 10 minutes allowed us to observe an appreciable fraction of the dynein ROIs become populated with BicD2 molecules (Fig. 4*D*). As expected, the k_{obs} determined for dynein-BicD2 in the 10- and 2-min experiments were the same (Fig. 4*C*). During this experiment, we also monitored dynactin binding and observed much faster association kinetics for dynactin than for BicD2 (Fig. 4*D*). The difference in dynein-dynactin and dynein-BicD2 association rates means that most complexes should form *via* dynactin-first binding, which we confirmed by directly monitoring the order of assembly for each tripartite complex (Fig. 4*E*). We were also able to observe a significant increase in the number of dynein-BicD2 and dynein-dynactin-BicD2 tripartite complexes that were long-lived, with 37% of dynein-BicD2 complexes and 35% of tripartite complexes surviving longer than 80 s (Figs. 4, *A* and *B* and S4, *D*–*H*). To ensure that the dynein-BicD2 binding we observed over 10 min was not the product of nonspecific interaction, we generated the $BicD2^{A/V}$ variant (which contains A43V and A44V mutations) that has been previously shown to disrupt binding to dynein light intermediate chain (6). We observed no binding between dynein and $BicD2^{A/V}$, while the dynein-dynactin association profiles in this context were the same as were observed with wild-type BicD2 (Fig. 4*F*). This confirms the specificity of the dynein-BicD2 interaction and shows that the dynein light intermediate chain plays a key role in dynein's ability to bind BicD2.

Altogether, the binding data collected with NINL and BicD2 show that because BicD2 binds dynein with significantly slower binding kinetics than NINL, dynein-dynactin-BicD2 complexes form much more slowly than complexes with NINL. Further, these complexes assemble primarily *via* dynactin binding first. However, once formed, the dynein-dynactin-BicD2 and dynein-dynactin-NINL complexes have comparable stabilities.

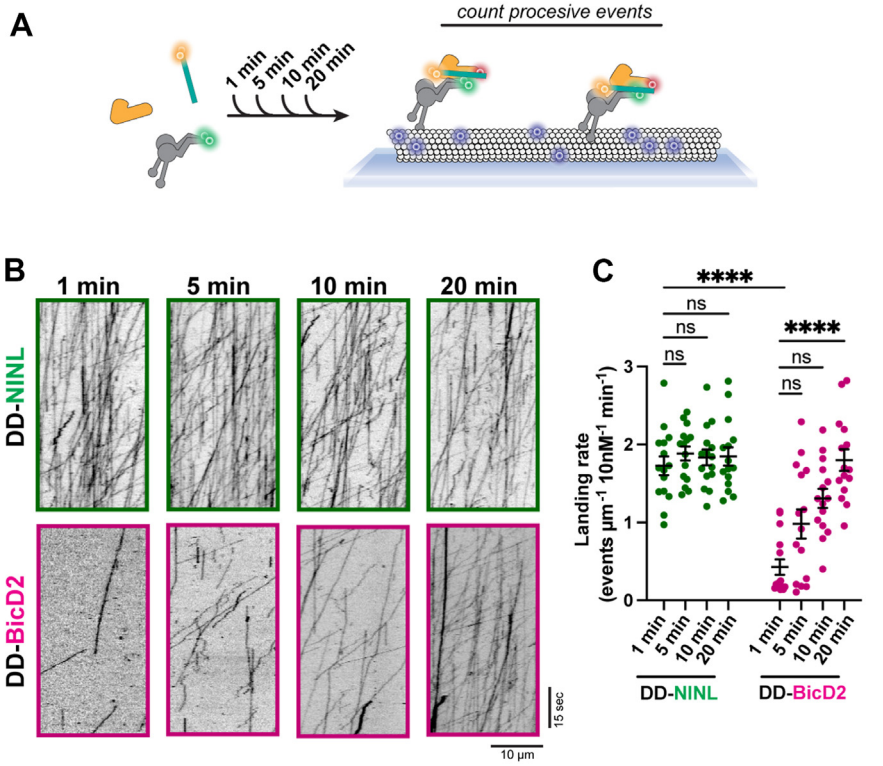

Figure 5. BicD2 activates dynein motility more slowly than NINL. *A*, diagram of a kinetic motility experiment in which dynein, dynactin and adaptor are incubated for 1, 5, 10, or 20 min before imaging dynein motility. *B*, example kymographs from the kinetic motility assay. *C*, landing rate of motile dynein-dynactin-NINL (*green*) or dynein-dynactin-BicD2 (*pink*) complexes. n = 15 microtubules. Statistical testing was performed with a Kruskal-Wallis test with Dunn's multiple comparisons test. ns $p > 0.05$, ****$p < 0.0001$.

Because NINL and BicD2 behave similarly in motility assays, these results were very surprising (16). However, motility studies that assess dynein activation are often performed after a 20-min incubation of dynein, dynactin, and adaptor (16). We reasoned that, by performing "kinetic motility" experiments in which the pre-incubation time of dynein, dynactin, and adaptor is varied, we should be able to directly observe the effects of assembly kinetics on dynein motility. To perform these experiments, we mixed dynein, dynactin, and adaptor proteins for between 1 min (the fastest we could mix the proteins and image) and 20 min; we then added ATP and imaged motility on Taxol-stabilized microtubules with TIRF microscopy. We assessed complex formation by determining the processive complex landing rate from the motility movies (Fig. 5*A*). Consistent with fast association, NINL's ability to generate activated transport complexes plateaued by the first time point (1 min), suggesting rapid complex formation (Fig. 5, *B* and *C*). In contrast, we observed results with BicD2 that were consistent with a dramatically slower association rate. With increasing incubation times, there was a clear increase in the amount of processive complexes formed, as measured by the landing rate (Fig. 5, *B* and *C*). By 20 min, BicD2 and NINL experiments had the same processive landing rate, which explains how the differences between the association kinetics of these adaptors previously eluded us (Fig. 5, *B* and *C*). Altogether, these data show that different adaptors can facilitate the assembly of activated complex formation with different kinetics. These differences also support the need to examine the dynamic process of dynein activation in pre-equilibrium conditions, as these adaptors don't diverge from each other dramatically once they have formed activated transport complexes.

Discussion

We set out to determine how dynein, dynactin, and cargo adaptors assemble into the activated transport complex. To accomplish this, we developed a single-molecule, TIRF-based assay that allowed us to measure the association kinetics of complex formation and visualize resultant complex stability. To our knowledge, this work is the first systematic effort to describe the dynamic, molecular processes that lead to dynein activation.

Using dynactin and the cargo adaptor NINL, we determined the mechanism by which the activated transport complex forms. We observed that bimolecular complexes (dynein-NINL and dynein-dynactin) were significantly shorter lived than the trimolecular dynein-dynactin-NINL complexes (Fig. 3, *A*–*F*). This observation may explain why only the dynein-dynactin-adaptor complexes (and not dynein-dynactin or dynein-adaptor complexes) are capable of processive motility (5, 6). For example, even if dynactin or NINL alone could promote a dynein conformation that is similar to the structure of dynein in active transport complexes, it is likely that the mechanical movements driven by ATP hydrolysis that power dynein stepping are sufficiently strong enough to destabilize the relatively weak bimolecular complexes. Additionally, it is possible that the difference in stabilities between bimolecular and trimolecular complexes could serve as a type of proofreading mechanism to ensure that dynein only enters a long-lived complex when both dynactin and an adaptor are present and capable of binding.

Our work also showed that the pairwise association of dynein with either dynactin or NINL are independent from each other. In other words, NINL and dynactin interact with free dynein at the same rate that they interact with dynein bound to the other partner, and complex formation can occur *via* dynactin or NINL binding first (Fig. 2, *E*–*G*). Additionally, the association rate constants of dynein-dynactin and dynein-NINL binding are similar to one another, meaning that at similar free concentrations, complex assembly will occur roughly equally by the two independent pathways (Fig. 3, *H* and *I*) Despite both pathways being available and their association rates being kinetically comparable, we observed that complexes formed *via* NINL-first events were more likely to be long-lived than complexes formed *via* dynactin-first events (Fig. 3, *E* and *F*).

Why might dynactin-first complexes be less likely to yield stable complexes? We reason that dynactin binding first can result in an "off-pathway" intermediate that has a greater probability of generating a complex with reduced stability. The contacts between dynein, dynactin, and an adaptor in the assembled activated transport complex are extensive and multivalent (7, 8, 11). Adaptors interact with dynein light intermediate chain through a domain at their N-terminus and interact with multiple sites on dynein heavy chain *via* an extended coiled coil (Fig. 1*A*) (7, 8, 11, 26–28). Adaptors also bind to dynactin's Arp filament with their coiled-coil and dynactin's pointed end complex *via* a short motif within the coiled-coil, called a spindly motif (29). Dynein and dynactin also have multiple points of contact. Dynein intermediate chain binds to a dynactin's p150 subunit and dynein heavy chain makes multiple sites of contact with dynactin subunits along the filament (Fig. 1*A*) (8, 30, 31). In the final active structure, the adaptor appears sandwiched between dynactin's Arp filament and the tails of the dynein heavy chain. We speculate that dynactin-first events may be prematurely "zipped-up" such that some of contacts between dynein heavy chain and dynactin form and disfavor or preclude adaptor insertion. In contrast, the binding of the adaptor to dynein may allow normal dynein-dynactin contacts to form, resulting in a higher probability of stable assembly when adaptors bind first. More work is required to understand complex assembly from a structural perspective, to determine which protein-protein contacts drive association, and to identify the structure of assembly intermediates.

Dynein molecules inside cells likely exist in multiple conformations because distinct populations of dynein are associated with microtubules and found throughout the cytoplasm. Cytoplasm-localized dynein is likely in the autoinhibited Phi conformation (Fig. 1*A*), and this structure is not compatible with high-affinity microtubule binding (10). It is unclear whether dynein destined for cargo trafficking is recruited from both pools, though experiments performed with purified

components show that the activated transport complex can form in solution (6). In this study, we employed the microtubule track to capture and stabilize dynein molecules. It is possible that the mechanism and kinetics of complex assembly of microtubule-bound dynein is distinct from that of cytoplasm-localized dynein. Developing methodology to determine the association kinetics of dyneins that are not associated with microtubules will be the focus of future work.

We also found that the adaptors NINL and BicD2 bind dynein with dramatically different association kinetics, which causes BicD2 to form activated transport complexes an order of magnitude slower than NINL. This also means that dynein-dynactin-BicD2 complexes assemble primarily through the dynactin-first pathway. Despite slower association kinetics, dynein-dynactin-BicD2 complexes can form structures that are stable and long-lived, as assessed by complex dwell time. We were also able to determine how differences in assembly kinetics manifested in traditional motility experiment readouts of dynein activation and found that dynein-dynactin-BicD2 complexes required significantly longer incubation times to yield activated transport complexes. These findings underscore how important it is to consider the kinetics of dynein binding to its regulatory partners when conducting traditional motility experiments.

The difference in assembly kinetics for complexes formed with NINL and complexes formed with BicD2 has potentially broad and significant implications. Dynein is tethered to its myriad cargos by one of nearly 20 different adaptors (4). It is not clear how dynein distinguishes between different cargo adaptors to traffic the appropriate cargo. Our work suggests that distinct association rates between dynein and different adaptors could be one mechanism by which dynein discriminates between adaptors to achieve trafficking specificity.

It is also possible that the differences in association rates between NINL and BicD2 have evolved as such to offset other kinetic processes that govern dynein's ability to traffic cargo. For example, both adaptor constructs used in this study are truncated, thus relieving potential autoinhibition. BicD2 is known to be autoinhibited and cannot associate with dynein when its C-terminal tail is folded back to interact with the N-terminal coiled-coil (15, 20). To facilitate switching between the folded, autoinhibited to open conformation, BicD2 binds to cargo-localized regulators, like Nup358 or Rab6 (15, 32–34). These same proteins promote BicD2's cargo localization, which means that BicD2 on cargo is likely in the open state that is competent to bind dynein. One could imagine that the slow association kinetics of dynein-BicD2 binding is essential for preventing excessive dynein activation on cargo that is laden with open BicD2. It is also possible that the differences in dynein-adaptor association kinetics have evolved to compensate for differences in adaptor concentration or accessibility. During interphase, NINL localizes primarily to the centrosome (35). It is unclear what the structure of NINL is at the centrosome, and thus, it is unclear whether dynein has access to all NINL molecules. Given the density and layered ultrastructure of the centrosome, it is possible that NINL is largely inaccessible to dynein and that rapid association kinetics ensures that the few accessible NINL molecules can drive activated transport complex formation (36).

By developing a novel *in vitro* assembly assay, we show that different adaptors bind to dynein with different kinetics, resulting in different assembly pathways for dynein-dynactin-adaptor complex formation. The present study sets the stage for a more complete accounting of how differences in adaptor association kinetics are harnessed by the cell to promote dynein's multiple functions. An important next step will be to determine the association rate constants for dynein's interaction with all other adaptors to fully map the kinetic parameters that govern dynein activation on different types of cargos.

Experimental procedures

Protein expression and purification

Dynein was expressed in Sf9 cells as described (25, 37). Briefly, human dynein genes in pACEBac1 plasmid were transformed into DH10EmBacY cells *via* 42 °C heat shock for 15 s followed by a 6 h outgrowth at 37 °C in S.O.*C. media* (Thermo Fisher Scientific) with shaking at 220 rpm. Cells were then plated on LB-agar containing kanamycin (50 μg/ml), gentamicin (7 μg/ml), tetracycline (10 μg/ml), BluoGal (100 μg/ml) and IPTG (40 μg/ml). After 48 to 72 h growth, white colonies were selected. Colonies were tested *via* PCR for the presence of all dynein genes. Selected colonies were grown 37 °C with shaking at 220 rpm in LB media with kanamycin (50 μg/ml), gentamicin (7 μg/ml) and tetracycline (10 μg/ml). After 14 to 16 h of growth, bacmid DNA was then extracted from cultures with isopropanol extraction. 1 to 2 μg of purified bacmid was transfected into 1×10^6 Sf9 cells with FuGene HD transfection reagent, according to manufacturer's instruction (Promega). Transfected cells were incubated in a six well dish at 27 °C without agitation for 3 days before 1 ml of supernatant (designated V0) from the transfected cells was collected *via* centrifugation (1000*g*, 5 min, 4 °C) and used to transfect of 50×10^6 SF9 cells/ml, in a final volume of 50 ml. Cells were agitated at 105 rpm at 27 °C for 3 days, before the supernatant (designated V1) was harvested *via* centrifugation. To express protein, 4 ml of V1 was used to transfect 400×10^6 SF9 cells/ml in a final volume of 400 ml and agitated at 105 rpm at 27 °C for 3 days. Cells were harvested *via* centrifugation, the pellet was washed with 10 ml of cold PBS, then frozen in liquid nitrogen and stored at −80 °C until needed for protein purification.

Purification of dynein was conducted as described (25, 37). All steps are performed at 4 °C unless otherwise noted. Briefly, dynein pellets were thawed on ice and resuspended in 40 ml per pellet of dynein-lysis buffer (50 mM HEPES (pH 7.4), 100 mM sodium chloride, 1 mM DTT, 0.1 mM Mg-ATP, 0.5 mM Pefabloc, 10% (v/v) glycerol) supplemented with cOmplete EDTA-free protease inhibitor cocktail (Roche). Lysis was accomplished *via* douncing and the lysate was clarified *via* centrifugation (183,960*g*, 88 min, 4 °C) in a Type 70Ti rotor (Beckman). 2 ml of IgG Sepharose 6 Fast Flow beads (Cytiva) were incubated with the clarified supernatant for 4 h with rotation. Beads were collected in a gravity column and washed

with at least 200 ml of dynein-lysis buffer and 300 ml of TEV buffer (50 mM Tris–HCl (pH 8.0), 250 mM potassium acetate, 2 mM magnesium acetate, 1 mM EGTA, 1 mM DTT, 0.1 mM Mg-ATP, 10% (v/v) glycerol). For fluorescent labeling, dynein-bound beads were mixed with 5 μM SNAP-Cell-TMR (for motility experiments) or SNAP-Alexa-488 (for kinetic binding experiments) (New England Biolabs) for 10 min at RT. Beads were then washed with 300 ml of TEV-buffer, then resuspended in 15 ml TEV buffer supplemented with 0.5 mM Pefabloc and up to 0.2 mg/ml TEV protease and incubated overnight with rotation. Cleaved proteins were separated from the beads with a gravity column and concentrated to 500 μl with a 100K MWCO concentrator (EMD Millipore). Dynein was then injected onto to TSKgel G4000SWXL column (Tosoh) equilibrated with GF150 buffer 25 mM HEPES (pH 7.4), 150 mM KCl, 1 mM $MgCl_2$, 1 mM DTT) supplemented with 0.1 mM Mg-ATP. Column was run at 0.75 ml/min, peak fractions were collected, buffer exchanged into GF150 buffer supplemented with 0.1 mg/ml ATP and 10% glycerol, concentrated to 0.1 to 0.5 mg/ml, flash frozen in small aliquots, and stored at −80 °C.

Dynactin was purified from HEK293T cells stably expressing p62-Halo-3xFLAG as described (17). Briefly, frozen pellets generated from 160 × 15 cm plates of ∼80% confluent cells were resuspended in 80 ml of of dynactin-lysis buffer (30 mM HEPES (pH 7.4), 50 mM potassium acetate, 2 mM magnesium acetate, 1 mM EGTA, 1 mM DTT, 10% (v/v) glycerol) supplemented with 0.5 mM Mg-ATP, 0.2% Triton X-100, and 1× cOmplete EDTA-free protease inhibitor cocktail tablets (Roche)). The lysate was clarified *via* centrifugation (66,000*g*, 30 min, 4 °C) in a Type 70 Ti rotor (Beckman), before being incubated overnight at 4 °C with 1.5 ml of anti-FLAG M2 affinity gel (Sigma-Aldrich) with rotation. Beads were collected with a gravity column, then washed with at least 50 ml of wash buffer (Dynactin-lysis buffer supplemented with 0.1 mM Mg-ATP, 0.5 mM Pefabloc and 0.02% Triton X-100), 100 ml of wash buffer supplemented with 250 mM potassium acetate, and then washed again with 100 ml of wash buffer. To fluorescently label dynactin, 5 μM HaloTag-Ligand conjugated TMR or JF646 (Promega) was added to the FLAG beads and incubated at room temperature for 10 min. The unconjugated dye was removed with an additional 100 ml of wash buffer. To elute dynactin, beads were incubated with 1 ml elution buffer (wash buffer with 2 mg/ml of 3xFlag peptide). Dynactin was then diluted to 2 ml in Buffer A (50 mM Tris-HCl (pH 8.0), 2 mM magnesium acetate, 1 mM EGTA, and 1 mM DTT) and loaded onto a MonoQ 5/50 Gl column (Cytiva) at 1 ml/min. A linear gradient from 35 to 100% Buffer B (50 mM Tris-HCl (pH 8.0), 2 mM magnesium acetate, 1 mM EGTA, 1 mM DTT, 1 M potassium acetate) was run over 26 column volumes. Fractions of pure dynactin that eluted between 75 to 80% Buffer B were collected, pooled, and buffer exchanged into GF150 buffer supplemented with 10% glycerol, concentrated to 0.02 to 0.1 mg/ml, flash frozen in small aliquots, then stored at −80 °C.

NINL (amino acids 1–702) and BicD2 (amino acids 1–598) constructs containing N-terminal HaloTags were expressed and purified as described (16, 25). Constructs were transformed into BL-21[DE3] cells (New England Biolabs) cells and cells were grown at 37 °C with shaking until they reached to an optical density at 600 nm of 0.4 to 0.6. Then the temperature was reduced to 18 °C and protein expression was induced with 0.1 mM IPTG for 16 h. Pellets were harvested *via* centrifugation, frozen, and stored at −80 °C until needed. All purification steps were performed at 4 °C, unless indicated otherwise. To purify either adaptor, pellets harvested from 1.5 L were thawed in 40 ml of adaptor-lysis buffer (30 mM HEPES pH 7.4, 50 mM potassium acetate, 2 mM magnesium acetate, 1 mM EGTA, 1 mM DTT and 0.5 mM Pefabloc, 10% (v/v) glycerol) supplemented with 1× cOmplete EDTA-free protease inhibitor cocktail tablets (Roche) and 1 mg/ml lysozyme. To lyse, cell slurry was sonicated then clarified *via* centrifugation (66,000*g* for 30 min) in Type 70 Ti rotor (Beckman). The supernatant was mixed with 2 ml of IgG Sepharose 6 Fast Flow beads (Cytiva) for 2 h with rotation before being washed with adaptor-lysis buffer supplemented with 150 mM potassium acetate and 50 ml of cleavage buffer (50 mM Tris-HCl pH 8.0, 150 mM potassium acetate, 2 mM magnesium acetate, 1 mM EGTA, 1 mM DTT, 0.5 mM Pefabloc and 10% (v/v) glycerol). The washed beads were then resuspended in 15 ml of cleavage buffer supplemented with 0.2 mg/ml TEV protease and incubated overnight with rotation. The supernatant containing the adaptor proteins was collected, concentrated to 1 ml with a 30 kDa MWCO concentrator (EMD Millipore), filtered, diluted to 2 ml in Buffer A (30 mM HEPES pH 7.4, 50 mM potassium acetate, 2 mM magnesium acetate, 1 mM EGTA, 10% (v/v) glycerol and 1 mM DTT) and injected into a MonoQ 5/50 Gl column (Cytiva) at 1 m/min. A linear gradient was run from 0 to 100% Buffer B (30 mM HEPES pH 7.4, 1 M potassium acetate, 2 mM magnesium acetate, 1 mM EGTA, 10% (v/v) glycerol and 1 mM DTT) over 26 column volumes. Peak fractions containing Halo-tagged adaptors were collected, concentrated to 0.2 ml, diluted to 0.5 ml in GF150 buffer and injected onto a Superose 6 Increase 10/300 Gl column (Cytiva) equilibrated with GF150 buffer. Column was run at 0.5 ml/min, peak fractions were collected, and buffer exchanged into GF150 buffer supplemented with 10% glycerol. To label adaptors, concentrated fractions were incubated with 5 μM HaloTag-Ligand conjugated TMR or JF646 (Promega) at room temperature for 10 min. Excess dye was removed with a Micro Bio-Spin desalting column preequilibrated with GF150 buffer supplemented with 10% glycerol. Proteins were flash frozen in small aliquots before being stored at −80 °C.

The concentrations of dynein, dynactin, NINL, and BicD2 were determined using densitometry analysis of SDS-PAGE gels with a standard curve generated from known quantities of bovine serum albumin. To determine how efficiently each protein sample was labeled with fluorescent dye, first the absorbance (at 494 nm for Alexa-488 labeled protein; 543 nm for TMR labeled protein; and 646 nm for JF646 labeled protein) was determined with a DeNovix DS-11 instrument. To calculate dye concentrations, the following extinction coefficients were used: 71,000 M^{-1} cm^{-1} for Alexa-488, 87,000

M^{-1} cm^{-1} for TMR, and 152,000 M^{-1} cm^{-1} for JF646. To determine labeling efficiency, the molar concentration of dye in each sample was divided by the molar concentration of protein (as determined by densitometry). We only used proteins that were labeled with greater than 95% efficiency for all kinetic binding experiments in this study.

Single-molecule TIRF microscopy

All single-molecule imaging experiments were performed on an inverted microscope (Nikon, Ti2-E Eclipse) with a 100×, 1.49 N A. oil immersion objective (Nikon, Apo) equipped with a LUNF-XL laser launch (Nikon) containing 405 nm, 488 nm, 561 nm, and 640 nm lasers. The excitation path was filtered through the appropriate quad bandpass filter cube (Chroma). The emission path was split with the appropriate dichroic mirror and filtered with appropriate emission filters (Chroma) using a W-View GEMINI image splitter (Hamamatsu). All emission signals were detected on an iXon Ultra 897 electron-multiplying CCD camera (Andor Technology). Microscopy controls and image acquisition were controlled with NIS Elements Advanced Research software (Nikon).

Motility assay and analysis

Motility experiments were performed in flow chambers assembled as described using No. 1-1/2 coverslips (Corning) functionalized with PEG-biotin (25, 38). 20 μM bovine tubulin (with ∼10% biotin-tubulin and ∼10% Alexa-488 tubulin) was polymerized for 30 min at 37 °C before being stabilized with 20 μM taxol. Flow chambers were assembled by first flowing in 1 mg/ml streptavidin in assay buffer (30 mM HEPES [pH 7.4], 2 mM magnesium acetate, 1 mM EGTA, 10% glycerol, 1 mM DTT, and 20 μM taxol) and incubating for 3 min. Next chambers were washed twice with 20 μl of assay buffer before a fresh dilution of taxol stabilized microtubules (final concentrations ∼0.1–0.4 μM) was flowed in and incubated for 3 min. Chambers were then washed twice with assay buffer supplemented with 1 mg/ml casein. To assemble dynein-dynactin-adaptor complexes, dynein (15 nM), dynactin, and the adaptor were mixed at a 1:2:10 M ratio and incubated for between 0 and 19 min. Immediately before imaging, the samples were mixed with assay buffer supplemented with 20 μM Taxol, 1 mg/ml casein, 71.5 mM β-mercaptoethanol, 0.05 mg/ml glucose catalase, 1.2 mg/ml glucose oxidase, 0.4% glucose, and 2.5 mM Mg-ATP. Samples were then introduced into the flow chamber and imaged immediately. Microtubules were imaged first by taking a single frame snapshot. Dynein (labeled with JF646) and adaptors (labeled with TMR) were imaged every 300 ms for 2 min. At the end of image acquisition, the microtubule channel was imaged once more to assess stage drift and movies showing drift were not used. Kymographs were generated from movies using ImageJ macros as described (39). Dynein landing rate was determined per microtubule according to the following equation: $landing\ rate = N_{pe}/(l_m \cdot [adaptor] \cdot t)$, where N_{pe} is the number of processive events, l_m is the microtubule length (in μm) and t is the length of the movie (in minutes). Only runs longer than eight pixels were included in the analysis. Bright protein aggregates, which were defined as molecules 4 times brighter than the background, were also excluded. All statistical analysis was performed in Prism10 (GraphPad).

Association assay

Association experiments were performed in custom-built flow chambers with ports on either end to allow the sample to be introduced during image acquisition. To make these flow chambers, 1.2 mm diameter holes were drilled into either side of a 1 mm glass slide (Fisher, 12-550-15). Flow chambers were constructed as above, with double-sided tape separating chambers with a hole on either end. The open ends of the chambers were sealed with epoxy (Devcon). 200 μl pipette tips were inserted into the holes and affixed with epoxy, after which 1.2 mm diameter (0.76 mm inner diameter) tubing was inserted into one of the pipette tips and affixed inside the pipette tip with epoxy. A 20-gauge needle on a 1 ml syringe was inserted into the tubing. To introduce sample into the flow chamber, the sample was pipetted into the pipette tip on the opposite end and the syringe was pulled back until all of the liquid flowed into the chamber.

To assemble chambers for the association experiments, 1 mg/ml streptavidin in assay buffer was incubated for 3 min before being washed out with assay buffer. Next, taxol stabilized Alexa-405 labeled microtubules were incubated for 3 min, before being washed out with assay buffer supplemented with 1 mg/ml casein. Dynein labeled with Alexa-488 was diluted to 25 to 100 pM in assay buffer with 1 mg/ml casein, supplemented with 0.025 U/ml apyrase, and then was flowed in and incubated for 10 min. The concentration of dynein in the chamber was calculated by taking the number of dynein spots in a field of view, dividing by Avogadro's number to get moles and then by the volume of a field of view to get molarity. The volume is calculated from the area of our field of view (81.92 × 40.96 μM) and the height of the double-sided tape we use to make chambers (76.2 μm) which gives 256 pL. A field of view with 150 dynein spots therefore has a dynein concentration of about 1 pM. The fields of view used ranged from 15 to 150 dynein spots. To monitor association, first a single snapshot of the dynein and microtubule channels were taken before the movie acquisition was started. Next, while imaging the appropriate channels, mixtures of dynactin and/or adaptors labeled with either TMR or JF646 (final concentrations between 5–10 nM) were introduced to the chamber. Movies were collected for 2 min total, with a frame rate of 150 ms/frame. For longer imaging performed with BicD2, movies were collected for 10 min with a frame rate of 750 ms/frame. In both cases, exposure times for each laser were 40 ms. At the end of the movie, another snapshot of the dynein and microtubule channels were acquired to assess stage movement and to ensure dynein molecules were still present.

Association assay considerations and analysis

Dynein molecules that were present in the first and last frames were set as regions of interest (ROIs) and circled with a

diameter of six pixels (0.942 μm). ROIs were assessed manually and those that contained bright puncta indicative of aggregates were not considered. Next, movies of the dynactin and adaptor channels were processed with a rolling ball background subtraction using a three-pixel radius. Next, traces of the intensity of dynactin or adaptor over time at dynein ROIs were generated and used for analysis. Using custom MATLAB scripts, we extracted kinetic parameters from each trace. These parameters include identity of first lander, event dwell time, and identity of first protein to dissociate. We also wrote a custom MATLAB script that automatically generated binding curves of the fraction of dynein ROIs per frame that were experiencing a dynactin or adaptor binding event for determining k_{obs} values (see below) (Fig. 1*C*). Binding events were defined as positive deviation from baseline intensity, which was set individually for dynactin and adaptor in each dataset. All ROIs were manually checked to determine if a second dynactin or adaptor molecule landed. Dynein ROIs that ever received a second, concurrent binding event were omitted from the analysis in case the ROIs contained two proximal dynein molecules. This occurred for 33% of the ROIs. While we acknowledge that it is possible for two adaptors to bind one dynein, we chose to only consider complexes with a single adaptor (see extended discussion below).

Another possible explanation for multiple dynactin or adaptor molecules appearing to localize simultaneously with one dynein ROI is interactions between dynactin or NINL and the microtubule. Indeed, the p150 subunit of dynactin has a microtubule binding domain and can diffuse along the microtubule track (40). To test the contribution of binding to microtubules, we flowed dynactin or NINL into chambers without dynein and found that the landing rate was 0.0053 events/μm/min/nM dynactin and 0.0041 events/μm/min/nM NINL. Based on the size of our ROIs and this observed landing rate, we would expect about 9.9% of our ROIs to erroneously include a dynactin event and 7.7% to include a NINL event. We conclude that two dynactin or adaptor binding events were likely caused by both two dynein molecules bound close together and interactions of dynactin and adaptor with the microtubule. Because only 2% of ROIs received neither dynactin or NINL, deleting ROIs that received two signals limited the contribution of nonspecific binding.

To calculate the photostability and blinking behavior of the fluorophores used in the association assay, we nonspecifically attached labeled dynactin and NINL to a coverslip and analyzed the fluorescent spots with the above framework. 67.3% of TMR dyes and 84.8% of JF646 dyes did not photobleach by the end of the imaging period (Fig. S1*G*). These values represent the lower limit of the fraction of fluorophores that remain excitable throughout the entirety of the 2-min imaging window. Because of the imaging modality used in this study, it is challenging to use these bleach rates to more formally normalize the collected binding data. We used TIRF imaging, which generates an excitation field of ∼200 nm; this represents ∼0.1% of the depth of the flow cell over a small fraction of the surface area. Because fluorophores are free to diffuse in and out of the TIRF field, the resulting bleaching of free fluorophores should be negligible. The bleaching probabilities do establish the upper boundary of error for identification of a terminal unbinding events (*i.e.* unbinding events that are not followed by a rebinding event), which is 32.7% and 15.2% for TMR and JF646, respectively, given the bleaching rates measured and described above.

Each fluorophore also blinked, which could make it challenging to differentiate an unbinding and rebinding event from a dye blink. To investigate how blinking behavior may impact our data, we plotted a frequency distribution of the time that each blinking event remained in the dark state for each dye. We determined that 60.9% (for TMR) and 79.9% (for JF646) of blinking events were shorter than 1.2 s (Fig. S1*F*). This finding motivated us to impose a 1.2 s (8 frames in the 2 min experiments) persistence cutoff, meaning that all events had to last longer than 1.2 s to be considered a *bona fide* binding or unbinding event. Though this means that we cannot accurately report on complexes that survive for less than 1.2 s, it increases confidence in our ability to differentiate unbinding from blinking in the data more generally. For example, consider a dynein ROI where we observe two binding events. With the imposed persistence cutoff applied and considering the likelihood of these fluorophores to blink within the 2-min acquisition window, the likelihood that this event is actually a single fluorophore transitioning from a bright to dark to bright state is 7.56% or 12.85%, for TMR and JF646, respectively (Fig. S1*H*; "blink" behavior). For 10-min experiments, we adjusted the cutoff to be four frames (equivalent to 3 s) and applied it in the same way. Further, to ensure that bleaching rates and blinking frequency differences between each dye did not interfere with our analysis, we collected at least one replicate of all NINL experiments with the fluorophore on dynactin and NINL swapped.

Association of dynactin or adaptor with dynein was assessed by the binding curves of the fraction of dynein ROIs bound as a function of time (18). k_{obs} was determined from each individual binding curve obtained with different NINL or dynactin concentrations in Prism10 (GraphPad) by fitting to the following equation: $y = y_0 + (y_{max} - y_0) * (1 - e^{-k_{obs} * t})$ (18, 19). Here, y_0 is the initial counts and y_{max} is the fraction dynein bound. Each k_{obs} value was plotted as a function of concentration and fit to a linear regression ($k_{obs} = k_{on}[A] + k_{off}$, where A is either NINL or dynactin). Association rate constants are given by the slope of this line (18, 19). While off-rates can correspond to the y-intercept of this line, it can be less accurate than a direct measure of off-rate (18). We instead calculated off-rates of dynactin and adaptor by dividing the total number of observed unbinding events by the summed dwell time of every binding event. This approach, which assumes dissociation events are history independent, takes into account binding events that are terminated by the end of the movie rather than an observed dissociation. Off-rates from the tripartite complex were calculated in the same way, by taking the number of unbinding events for either dynactin or adaptor and dividing by the summed dwell time of all tripartite complexes. Probability density functions of dwell times were generated in MATLAB with a Gaussian mixture model script.

The number of Gaussians that best fit the data was determined using Bayesian information criterion. The maximum number of Gaussians tested was 6.

Protein aggregation or oligomerization before binding a dynein ROI could complicate our ability to reliably interpret the data collected. To ensure that the majority of our binding events reflect the behavior of a single dynein dimer interacting with a single dynactin and/or dimeric adaptor, we generated histograms of the intensity of each spot for dynein, dynactin, and NINL in the experimental condition with the most bioreplicates (the condition with 10 nM dynactin and 10 nM NINL). Though these distributions are expected to be wide because of nonhomogeneous illumination across the field of view and slight variations in the TIRF angle between experiments, the shape of the distributions are useful in assessing the presence of higher order oligomers or aggregates.

For the dynein distribution, we plotted the first frame intensity of all dynein spots used for analysis (Fig. S1*A*). Dynein was only labeled with Alexa-488. In our imaging conditions, the mean intensity of free Alexa-488 was 91.2 ± 29.6 (error is standard deviation) (Fig. S1*A*, yellow box). Nearly all dynein ROIs have intensities that correspond to either one or two fluorophores, indicating a dimer that has one or two monomers labeled (Fig. S1*A*).

For dynactin and NINL, we plotted the average intensity of the signal for the duration of time that each component was present at a dynein ROI. Some experiments had dynactin labeled with JF646 and NINL labeled with TMR, while some had the fluorophores swapped. We assessed the intensity of each protein with either dye separately. In our imaging conditions, the mean intensity of free JF646 was 86.5 ± 39.2 and free TMR was 52.6 ± 20.8 (Fig. S1, *B–E*, yellow boxes). 71% dynactin-646 and 82% of dynactin-TMR events corresponded to intensities that correspond to one fluorophore (which is expected as only one copy of p62 is found in the dynactin complex) (Fig. S1, *B* and *C*). 29% and 18% of dynactin-646 and dynactin-TMR had intensities closer to that of two fluorophores (Fig. S11, *B* and *C*). This population likely reflects dynactin molecules that received two fluorophores, rather than dynactin dimers because for a few of our preps, we observed dynactin labeling efficiency that was greater than 100% (indicating that some dynactin molecules have dye nonspecifically attached). 98% of NINL-646 have intensity values that correspond to two fluorophores (as expected for a dimer) (Fig. S1*D*).∼59% and 41% of NINL-TMR events have intensity levels that correspond to two or one fluorophore, respectively, suggesting that one fluorophore on a population of adaptors gets bleached (Fig. S1*E*).

Experimental limitations and caveats

The association experiments we have designed explicitly monitor the association of one dynein dimer with one dynactin complex and one dimeric adaptor, as described above. It is important to emphasize that activated transport complexes often contain two dynein dimers and can also contain two adaptor dimers (7, 8). To our knowledge, this work represents the first effort towards determining the order of events that precede complex formation, therefore it is not clear if a dynein dimer must bind dynactin and a single adaptor dimer before the second dynein and adaptor are recruited or if these binding events can occur randomly. Determining the sequence of assembly of these higher-order complexes in the future would require, for instance, immobilizing an adaptor and monitoring binding of dynein, dynactin, and an additional adaptor molecule.

Additionally, it is not clear where in the cell the activated transport complex forms. While populations of dynein and dynactin do reside on the microtubule plus-end, the structure of these proteins and how they bind the microtubule is not known (20). There are also populations of dynein and dynactin present in the cytoplasm, not associated with microtubules (20). In this study, we used the microtubule track to immobilize dynein and observe association with dynactin and adaptors. The binding observed in this study may not reflect the behavior of how preformed complexes of dynein-dynactin on the microtubule interact with adaptor or how cytoplasm-localized dynein interacts with dynactin and adaptors.

Finally, the dwell times measured in this study, particularly for tripartite complexes, are relatively long-lived, especially compared to the duration of the experiments. Indeed, more than half of all dynein-dynactin-NINL binding events observed were terminated by the end of data acquisition rather than complex dissociation. Even when imaging conditions were extended to 10 min for BicD2 binding, tripartite complexes were formed that lasted longer than the duration of the experiment. This means that our calculated off-rates may be overestimations of true off rates.

Equilibrium binding experiments

The binding of dynein, dynactin and NINL was measured in solution by coupling 100 nM NINL to 35 µl of NEBExpress Ni-NTA Magnetic Beads (NEB) in the case of NINL-dynactin binding or 100 nM dynein to 25 µl SNAP-Capture Magnetic Beads (NEB) in 2 ml Protein Lo Bind Tubes (Eppendorf) using the following protocol. Beads were washed twice with 1 ml of GF150 without ATP supplemented with 10% glycerol and 0.1% NP40. NINL or Dynein was diluted in this buffer to 100 nM. 25 µl of diluted protein was added to the beads and gently shaken for 1 hour. 20 µl of the supernatant were then analyzed *via* SDS-PAGE to confirm complete depletion of the protein by the beads. The protein-conjugated beads were washed once with 1 ml GF150 with 10% glycerol and 0.1% NP40 and once with 1 ml of binding buffer (28.75 mM HEPES [pH 7.4], 1.5 mM magnesium acetate, 0.75 mM EGTA, 0.25 mM $MgCl_2$, 37.5 mM KCl, 10% glycerol, 1 mM DTT, 1 mg/ml casein, 0.1% NP40, 1 mM ADP). 5 nM dynactin or NINL was diluted such that the final buffer composition was binding buffer. 25 µl of the dynactin or NINL mixture was added to the beads and gently agitated for 45 min. After incubation 20 µl of the supernatant was removed, and 6.67 µl of NuPAGE LDS Sample Buffer (4×) and 1.33 µl of Beta-mercaptoethanol was added to

each. The samples were boiled for 5 min before running on a 4 to 12% NuPAGE Bis-Tris gel. Depletion was determined using densitometry in ImageJ.

Data availability

All custom scripts will be available on github.com/DeSantis-Lab. All data will be made available upon request. Please direct requests to mdesant@umich.edu.

Supporting information—This article contains supporting information.

Acknowledgments—The authors thank Drs. Michael Cianfrocco, David Sept, Patrick O'Brien, Kristen Verhey, and Randy Stockbridge as well members of the DeSantis, Cianfrocco, Verhey, Ohi, Sept, and Hancock labs for helpful discussions and/or feedback on the manuscript.

Author contributions—J. P. G., W. O. H., S. R. L. A. S., and M. E. D. writing–review & editing; J. P. G., M. E. D., and W. O. H. visualization; J. P. G. and M. E. D. project administration; J. P. G., M. E. D., and W. O. H. methodology; J. P. G., A. S., M. E. D., and S. R. L. investigation; J. P. G., A. S., M. E. D., W. O. H., and S. R. L. formal analysis; J. P. G. and M. E. D. conceptualization; A. S. and S. R. L. validation;. M. E. D. writing–original draft; M. E. D. supervision; M. E. D. resources; M. E. D. funding acquisition.

Funding and additional information—This work was supported by NIH-R35GM146739 and NSF-2142670 (to M. E. D.) and NIH-R35GM139568 (to W. O. H.).

Conflicts of interests—The authors declare that they have no conflicts of interest with the contents of this article.

Abbreviations—The abbreviations used are: dyenin, Cytoplasmic dynein-1; NEB, Ni-NTA Magnetic Beads; ROI, regions of interest; TIRF, Total Internal Reflection Fluorescence.

References

1. Cianfrocco, M. A., DeSantis, M. E., Leschziner, A. E., and Reck-Peterson, S. L. (2015) Mechanism and regulation of cytoplasmic dynein. *Annu. Rev. Cell Dev. Biol.* **31**, 83–108
2. Canty, J. T., Tan, R., Kusakci, E., Fernandes, J., and Yildiz, A. (2021) Structure and mechanics of dynein motors. *Annu. Rev. Biophys.* **50**, 549–574
3. Wickstead, B. (2018) 3 - the evolutionary biology of dyneins. In: King, S. M., ed. *Dyneins: Structure, Biology and Disease*, Second Edition, Academic Press: 100–138. https://doi.org/10.1016/B978-0-12-809471-6.00003-6
4. Reck-Peterson, S. L., Redwine, W. B., Vale, R. D., and Carter, A. P. (2018) The cytoplasmic dynein transport machinery and its many cargoes. *Nat. Rev. Mol. Cell Biol.* **19**, 382–398
5. McKenney, R. J., Huynh, W., Tanenbaum, M. E., Bhabha, G., and Vale, R. D. (2014) Activation of cytoplasmic dynein motility by dynactin-cargo adapter complexes. *Science* **345**, 337–341
6. Schlager, M. A., Hoang, H. T., Urnavicius, L., Bullock, S. L., and Carter, A. P. (2014) In vitro reconstitution of a highly processive recombinant human dynein complex. *EMBO J.* **33**, 1855–1868
7. Urnavicius, L., Lau, C. K., Elshenawy, M. M., Morales-Rios, E., Motz, C., Yildiz, A., and Carter, A. P. (2018) Cryo-EM shows how dynactin recruits two dyneins for faster movement. *Nature* **554**, 202–206
8. Chaaban, S., and Carter, A. P. (2022) Structure of dynein-dynactin on microtubules shows tandem adaptor binding. *Nature*. https://doi.org/10.1038/s41586-022-05186-y
9. Carter, A. P., Diamant, A. G., and Urnavicius, L. (2016) How dynein and dynactin transport cargos: a structural perspective. *Curr. Opin. Struct. Biol.* **37**, 62–70
10. Zhang, K., Foster, H. E., Rondelet, A., Lacey, S. E., Bahi-Buisson, N., Bird, A. W., and Carter, A. P. (2017) Cryo-EM reveals how human cytoplasmic dynein is auto-inhibited and activated. *Cell* **169**, 1303–1314.e18
11. Singh, K., Lau, C. K., Manigrasso, G., Gama, J. B., Gassmann, R., and Carter, A. P. (2024) Molecular mechanism of dynein-dynactin complex assembly by LIS1. *Science* **383**, eadk8544
12. Bachmann-Gagescu, R., Dona, M., Hetterschijt, L., Tonnaer, E., Peters, T., de Vrieze, E., *et al.* (2015) The ciliopathy protein CC2D2A associates with NINL and functions in RAB8-MICAL3-regulated vesicle trafficking. *PLoS Genet.* **11**, e1005575
13. Yin, L., Coelho, S. G., Ebsen, D., Smuda, C., Mahns, A., Miller, S. A., *et al.* (2014) Epidermal gene expression and ethnic pigmentation variations among individuals of Asian, European and African ancestry. *Exp. Dermatol.* **23**, 731–735
14. Cui, H., Ali, M. Y., Goyal, P., Zhang, K., Loh, J. Y., Trybus, K. M., and Solmaz, S. R. (2020) Coiled-coil registry shifts in the F684I mutant of Bicaudal D result in cargo-independent activation of dynein motility. *Traffic* **21**, 463–478
15. Gibson, J. M., Cui, H., Ali, M. Y., Zhao, X., Debler, E. W., Zhao, J., *et al.* (2022) Coil-to-α-helix transition at the Nup358-BicD2 interface activates BicD2 for dynein recruitment. *eLife* **11**, e74714
16. Htet, Z. M., Gillies, J. P., Baker, R. W., Leschziner, A. E., DeSantis, M. E., and Reck-Peterson, S. L. (2020) LIS1 promotes the formation of activated cytoplasmic dynein-1 complexes. *Nat. Cell Biol.* **22**, 518–525
17. Redwine, W. B., DeSantis, M. E., Hollyer, I., Htet, Z. M., Tran, P. T., Swanson, S. K., *et al.* (2017) The human cytoplasmic dynein interactome reveals novel activators of motility. *Elife* **6**, e28257
18. Pollard, T. D., and De La Cruz, E. M. (2013) Take advantage of time in your experiments: a guide to simple, informative kinetics assays. *Mol. Biol. Cell* **24**, 1103–1110
19. Hoare, S. R. J. (2004) Analyzing kinetic binding data. In: Markossian, S., *et al.* eds. *Assay Guidance Manual*, Eli Lilly & Company and the National Center for Advancing Translational Sciences, Bethesda (MD)
20. Splinter, D., Razafsky, D. S., Schlager, M. A., Serra-Marques, A., Grigoriev, I., Demmers, J., *et al.* (2012) BICD2, dynactin, and LIS1 cooperate in regulating dynein recruitment to cellular structures. *MBoC* **23**, 4226–4241
21. Splinter, D., Tanenbaum, M. E., Lindqvist, A., Jaarsma, D., Flotho, A., Yu, K. L., *et al.* (2010) Bicaudal D2, dynein, and kinesin-1 associate with nuclear pore complexes and regulate centrosome and nuclear positioning during mitotic entry. *PLoS Biol.* **8**, e1000350
22. Hu, D. J.-K., Baffet, A. D., Nayak, T., Akhmanova, A., Doye, V., and Vallee, R. B. (2013) Dynein recruitment to nuclear pores activates apical nuclear migration and mitotic entry in brain progenitor cells. *Cell* **154**. https://doi.org/10.1016/j.cell.2013.08.024
23. Hoogenraad, C. C., and Akhmanova, A. (2016) Bicaudal D family of motor adaptors: linking dynein motility to cargo binding. *Trends Cell Biol.* **26**, 327–340
24. Hoogenraad, C. C., Akhmanova, A., Howell, S. A., Dortland, B. R., De Zeeuw, C. I., Willemsen, R., *et al.* (2001) Mammalian Golgi-associated Bicaudal-D2 functions in the dynein-dynactin pathway by interacting with these complexes. *EMBO J.* **20**, 4041–4054
25. Garrott, S. R., Gillies, J. P., Siva, A., Little, S. R., El Jbeily, R., and DeSantis, M. E. (2023) Ndel1 disfavors dynein–dynactin–adaptor complex formation in two distinct ways. *J. Biol. Chem.* **299**, 104735
26. Lee, I.-G., Cason, S. E., Alqassim, S. S., Holzbaur, E. L. F., and Dominguez, R. (2020) A tunable LIC1-adaptor interaction modulates dynein activity in a cargo-specific manner. *Nat. Commun.* **11**, 5695
27. Celestino, R., Henen, M. A., Gama, J. B., Carvalho, C., McCabe, M., Barbosa, D. J., *et al.* (2019) A transient helix in the disordered region of dynein light intermediate chain links the motor to structurally diverse adaptors for cargo transport. *PLoS Biol.* **17**, e3000100

28. Lee, I.-G., Olenick, M. A., Boczkowska, M., Franzini-Armstrong, C., Holzbaur, E. L. F., and Dominguez, R. (2018) A conserved interaction of the dynein light intermediate chain with dynein-dynactin effectors necessary for processivity. *Nat. Commun.* **9**, 986
29. Gama, J. B., Pereira, C., Simões, P. A., Celestino, R., Reis, R. M., Barbosa, D. J., *et al.* (2017) Molecular mechanism of dynein recruitment to kinetochores by the Rod–Zw10–Zwilch complex and Spindly. *J. Cell Biol.* **216**, 943–960
30. Okada, K., Iyer, B. R., Lammers, L. G., Gutierrez, P. A., Li, W., Markus, S. M., and McKenney, R. J. (2023) Conserved roles for the dynein intermediate chain and Ndel1 in assembly and activation of dynein. *Nat. Commun.* **14**, 5833
31. Jie, J., Löhr, F., and Barbar, E. (2017) Dynein binding of competitive regulators dynactin and NudE involves novel interplay between phosphorylation site and disordered spliced linkers. *Structure* **25**, 421–433
32. Matsuto, M., Kano, F., and Murata, M. (2015) Reconstitution of the targeting of Rab6A to the Golgi apparatus in semi-intact HeLa cells: a role of BICD2 in stabilizing Rab6A on Golgi membranes and a concerted role of Rab6A/BICD2 interactions in Golgi-to-ER retrograde transport. *Biochim. Biophys. Acta* **1853**, 2592–2609
33. Tsai, M.-H., Cheng, H. Y., Nian, F. S., Liu, C., Chao, N. H., Chiang, K. L., *et al.* (2020) Impairment in dynein-mediated nuclear translocation by BICD2 C-terminal truncation leads to neuronal migration defect and human brain malformation. *Acta Neuropathologica Commun.* **8**, 106
34. Gonçalves, J. C., Quintremil, S., Yi, J., and Vallee, R. B. (2020) Nesprin-2 recruitment of BicD2 to the nuclear envelope controls dynein/kinesin-mediated neuronal migration in vivo. *Curr. Biol.* **30**, 3116–3129.e4
35. Jin, S., Gao, H., Mazzacurati, L., Wang, Y., Fan, W., Chen, Q., *et al.* (2009) BRCA1 interaction of centrosomal protein Nlp is required for successful mitotic progression. *J. Biol. Chem.* **284**, 22970–22977
36. Pereira, S. G., Louro, M. A. D., and Bettencourt-Dias, M. (2021) Biophysical and quantitative principles of centrosome biogenesis and structure. *Annu. Rev. Cell Dev. Biol.* **37**, 43–63
37. Agrawal, R., Gillies, J. P., Zang, J. L., Zhang, J., Garrott, S. R., Shibuya, H., *et al.* (2022) The KASH5 protein involved in meiotic chromosomal movements is a novel dynein activating adaptor. *eLife* **11**, e78201
38. Case, R. B., Pierce, D. W., Hom-Booher, N., Hart, C. L., and Vale, R. D. (1997) The directional preference of kinesin motors is specified by an element outside of the motor catalytic domain. *Cell* **90**, 959–966
39. Roberts, A. J., Goodman, B. S., and Reck-Peterson, S. L. (2014) Reconstitution of dynein transport to the microtubule plus end by kinesin. *eLife* **3**, e02641
40. Culver–Hanlon, T. L., Lex, S. A., Stephens, A. D., Quintyne, N. J., and King, S. J. (2006) A microtubule-binding domain in dynactin increases dynein processivity by skating along microtubules. *Nat. Cell Biol.* **8**, 264–270

John P. Gillies is a senior research lab specialist at the University of Michigan, where he studies the regulation of the microtubule-associated motor, dynein. He is fascinated by the many roles that this protein has in the cell and aims to understand the network of regulation that makes them all possible.

Saffron Little is an Entrepreneurial Fellow at the Chicago Biomedical Consortium through Northwestern University, a program fostering emerging biotech leaders to bridge academic breakthroughs and commercialization. She earned her PhD in Chemical Biology from the University of Michigan, where she developed microscopy assays to study the dynein transport complex. Now, she focuses on transforming scientific discoveries into real-world innovations. LinkedIn: www.linkedin.com/in/saffronlittle.